ESJ Humanities Peer-reviewed

Integrated Morphometric and Pedological Approach for Mapping Groundwater Availability Potential of Urban Watersheds: Case Study of the Former Municipality of Ratoma (Guinea)

Tokpo Ninamou
Laboratory of Science and Technology of Water and the Environment (LSTEE), National Institute of Water (INE), African Centre of Excellence for Water and Sanitation (C2EA),
University of Abomey-Calavi (UAC), Cotonou, Benin
Hydraulics Laboratory of the Small Hydropower Technology Center
University Gamal Abdel Nasser of Conakry, Guinea
Elegbede Manou Bernadin, MC
Laboratory of Science and Technology of Water and the Environment (LSTEE), National Institute of Water (INE), African Centre of Excellence for Water and Sanitation (C2EA),
University of Abomey-Calavi (UAC), Cotonou, Benin
Kourouma Mory, MA
Applied Research Laboratory in Geoscience and Environnement,
Institute of Mines and Geology of Boké (ISMGB), Guinea
NTcha Tchantipe
Laboratory of Science and Technology of Water and the Environment (LSTEE), National Institute of Water (INE), African Centre of Excellence for Water and Sanitation (C2EA),
University of Abomey-Calavi (UAC), Cotonou, Benin
Pr. Sine Diakite
Urban Study and Research Laboratory (LERU),
Higher Institute of Architecture and Urban Planning, Guinea

Doi:10.19044/esj.2026.v22n11p73

Submitted: 19 November 2025
Accepted: 23 April 2026
Published: 30 April 2026

Cite As:
Ninamou, T., Elegbede, M.B., Kourouma, M., Ntcha, T., & Diakite, S. (2026). *Integrated Morphometric and Pedological Approach for Mapping Groundwater Availability Potential of Urban Watersheds: Case Study of the Former Municipality of Ratoma (Guinea)*. European Scientific Journal, ESJ, 22 (11), 73. https://doi.org/10.19044/esj.2026.v22n11p73

ISSN: 1857-7881 (Print)
e-ISSN 1857-7431 (Online)

Abstract

To address water supply challenges in urban zones, this study proposes an integrated approach to characterize the water availability potential of the watersheds in the municipality of Ratoma in Guinea. This work combines remote sensing, Geographic Information Systems, pedology, and multivariate statistical analysis. Based on the DTM, 38 watersheds were characterized based on 23 morphometric parameters. Principal Component Analysis explained 72,92% of the total variance across three axes: size and drainage (39,86%), relief energy (18,79%), and the shape and compactness axis (14,28%). Hierarchical ascending classification identified two functional groups: small basins (0,16-1,67 km²) with rapid hydrological response, and larger basins (1,76-7 km²) with slower dynamics. Simultaneously, pedological analysis identified nine soil units, dominated by skeletal formations (75%) with rapid drainage. Soil granulometric analysis revealed textural variability that can influence infiltration. Coarse soils have high infiltration capacity but low water retention, while fine soils display temporary hydromorphism. Combining the results allowed for the spatial identification of areas with high water potential (hydromorphic soils) and transit areas (skeletal soils). Nevertheless, the hydrological responses remain hypothetical and do not allow for the establishment of predictive capacities for flow rates or recharge. Therefore, hydrogeological investigations remain necessary to refine the methodological approach used in order to produce a decision-making tool for the sustainable management and planning of water resources, facilitating the choice of drilling sites.

Keywords: Urban watershed, Remote sensing, Morphometry, Statistical analysis, Water potential

1. Introduction

Improving access to safe drinking water for populations living in urban and peri-urban areas, particularly through the development of water points such as boreholes, enables communities to obtain a reliable and sustainable water supply. The success and long-term sustainability of these groundwater sources primarily depend on selecting an appropriate site.

To identify the most suitable location, several interdependent factors must be considered, including resource availability, accessibility, and exploitability. In this study, “availability” refers to parameters such as drainage, slope, infiltration, and landform characteristics. Therefore, a morphometric and pedological characterization of the study area watersheds is required.

By definition, a watershed is a land area drained by a main stream and its tributaries. According to Polidori L. (1997), a watershed results from the

ISSN: 1857-7881 (Print)
e-ISSN 1857-7431 (Online)

interaction between a rainfall field and the land surface. The USGS (2019) views watersheds in terms of water reservoir development, while UNESCO-IHP (1973) proposed adapted approaches for watershed characterization. Kirsten Hennrich (2004) describes the watershed as a functional unit for hydrological research by introducing integrated management. Michel Lang (2015) defines a watershed as the region where all flows from rainfall, groundwater, or glacier melt accumulate and converge toward a specific outlet, bounded by ridgelines that delimit the actual drainage zone.

Watershed morphology analysis relies on field observations, maps, and satellite data. Key influencing factors include land use, soil lithology, vegetation cover, climate, runoff intensity, and hydrological risks; their interaction explains watershed hydrological behavior (Baba-Hamed, 2016). In urban settings, unplanned construction and soil sealing strongly alter hydrological regimes and increase flood risks (Desbordes, 1989). Recent work by Cyrus Omwoyo Ongaga (2024) shows that quantifying imperviousness shortens the concentration time and disrupts the hydrological cycle.

The objective of the article is to employ remote sensing data to analyze hydromorphometric parameters by integrating with pedological characteristics, which influence hydrology, to estimate zones of relative groundwater potential within watersheds. Satellite imagery provides continuous spatiotemporal data over the study area. The collected information was processed using statistical methods to classify watersheds into homogeneous groups according to their physical and hydrological characteristics.

2. Methodology and materials used

2.1. Study Area

Located between latitudes 9°34′N – 9°42′N and longitudes 13°32′W – 13°40′W, Ratoma covers 62,12 km² in the north to northwest of Conakry, bordered by the Atlantic Ocean to the north, the commune of Dubreka to the east, Matoto to the southeast, and Dixinn to the west. Topography ranges from 0 to 130 m in elevation, with flat terraces at approximately 20m altitude and slope descending gently toward the Kakoulima Mountains which peak at 10007m. Transverse depressions channel predominantly seasonal watercourses from the ridgeline toward the coast. While the hydrographic network consists of marigots and lakes. The dominant relief type is erosional and erosion-denudation. Ratoma experiences a subtropical climate with alternating dry and rainy seasons, governed by monsoon winds. Vegetation is limited to the Kakimbo forest (Sylla Morciré, 1995). Following FAO (2016) field soil description procedure, Ratoma soils are classified as azonal.

ISSN: 1857-7881 (Print)
e-ISSN 1857-7431 (Online)

2.2. Data and materials

Data used comprise a Digital Elevation Model (DEM), Google Earth imagery and OpenStreetMap imagery, 1:50 000 topographic map, mobile GPS, pedological data and SPSS, ArcGIS, QGIS and GlobalMapper for analysis of watershed delineation, spatial processing, and evaluation of hydro-morphometric parameters and groundwater-related characteristics, following approaches validated by Bentekhici N. (2006), Baba Hamed & Bounani (2016), and Lakraa (2022).

2.3. Methods

For characterizing the Ratoma watersheds, we adopted their definition and function (USGS, 2019). This characterization relies on an integrated approach combining geospatial and pedological analyses, structured into five stages following FAO (2023) and USGS (2019) guidelines. It integrates GIS tools, satellite DEM data and multivariate statistical methods to identify controlling parameters and assess groundwater potential.

2.3.1. Use of satellite imagery: Satellite imagery constituted our primary data source, enabling mapping of inaccessible areas. The raster derived from Landsat 8 characterized the current terrain morphology. Following Ahmad Badruzzaman et al. (2025), satellite image processing and feature extraction methods were applied. In this study, parameter determination followed a structured procedure outlined accordingly:

Step 1: watershed delineation and hydrographic network extraction were performed using a DEM derived from SRTM data (30 m resolution) downloaded from the USGS platform. Processing in QGIS enables the extraction of flow direction, flow accumulation, and associated watersheds boundaries, following the methodology outlined by the USGS (2019).

Step 2: It concerns the morphometric analysis, aiming to compute shape and network parameters following the methods described in Horton R. E. (1932, 1945) and Strahler (1957). Table 1 presents the calculation methods used for steps 1 and 2 based on empirical formulas.

Table 1: Methods for determining characteristic parameters of watersheds

Morphometric parameters	Methods	References
Geometric parameters		
Watershed area (A)	Automatic extraction by Arc Hydro from Argis	(Schumm S.A., 1956)
Watershed perimeter (P)	Automatic extraction by Arc Hydro de Argis	
Gravelius compactness coefficient (*This coefficient is used to assess the circularity of a watershed.)*	$K_G = \frac{P}{2\sqrt{\pi A}} = 0{,}28 \times \frac{P}{\sqrt{A}}$ *K_G − Gravelius compactness index; P − Watershed perimeter (km); A − Watershed area (km²).*	(Horton Robert E., 1945)

ISSN: 1857-7881 (Print)
e-ISSN 1857-7431 (Online)

Equivalent rectangle *(Used to assess the influence of watershed geometry on surface runoff)*	$L_r = \frac{K_G\sqrt{A}}{1{,}12} \times \left[1 + \sqrt{1 - \left(\frac{1{,}12}{K_G}\right)^2}\right]$ L_r − Length of the equivalent rectangle (km);K_G − Gravelius compactness index;A − Watershed area (km²).	(Horton Robert E., 1945)
Relief parameters of watersheds		
Maximum altitude (*The maximum altitude corresponds to the highest point in the watershed*)	Analysis of the topographic map	
Minimum altitudes (*The minimum altitude indicates the lowest point of the BV*)	Analysis of the topographic map	
Median elevation *(This is the elevation read at the point with an abscissa of 50% of the total area of the BV, on the hypsometric curve)*	Altitude at the abscissa point 50% of the total area of the BV	(Schumm S.A., 1956)
Average elevation *(This is deduced directly from the hypsometric curve or from reading a topographic map.)*	$H_{moy} = \sum \frac{A_i \times h_i}{A}$ H_{moy} − average altitude (m);A_i − Area of each altitude range (km²);h_i − average altitude of each range (m);A − Total area of the BV (km²).	
Average slope *(The average slope is a parameter that provides information about the topography of the basin)*	$i_m = \frac{D \times L}{A}$:i_m − Average slope (m/km or %); L− Total length of all contour lines (km);A − Total area of the watershed (km²);D − Equidistance between two contour lines (m).	(Cartier L. et Leclerc A., 1964)
Average slope index *(Ratio between the difference in extreme altitudes and the length of the equivalent rectangle)*	$I_{pm} = \frac{(H_{max} - H_{min})}{Lr} = \frac{\Delta H}{Lr}$ I_{pm} − Average slope index (m/km or %); Lr − length of the equivalent rectangle (km);H_{max} − maximum altitude (m); H_{min} − minimum altitude (m).	
Overall gradient index *(This is the ratio between the overall elevation gain and the length of the equivalent rectangle)*	$I_{pg} = \frac{D_g}{Lr}$ I_{pg} − Overall gradient index (m/km); Lr − length of the equivalent rectangle (km);D_g − Overall elevation gain (m).	(Sorre Maximilien, 1934)
Roche slope index *(Sum of the square roots of the average slopes of each partial element between two contour lines, weighted by the partial area associated with it and measured on the equivalent rectangle)*	$I_{pr} = \frac{1}{\sqrt{Lr}} \sum \sqrt{a_i . d_i}$ Where:I_{pr} − Slope index of rock (%) ; Lr − length of the equivalent rectangle (km) ;a_i − percentage of the area between the contour lines ;d_i − distance between the contour lines (m).	(Cartier L. et Leclerc A., 1964)

ISSN: 1857-7881 (Print)
e-ISSN 1857-7431 (Online)

Overall elevation difference *(Taken from the hypsometric curve, this is the difference between the upstream altitude and the downstream altitude)*	$D_g = H_{5\%} - H_{95\%}$ Where:D_g − Total elevation difference (m);$H_{5\%}$ − altitude corresponding to 5% of the total area of the watershed (m);$H_{95\%}$ − altitude corresponding to 95% of the total area of the watershed (m).	(Cartier L. et Leclerc A., 1964)
Specific elevation difference *(Allows comparison of watersheds of different sizes)*	$D_S = I_{pg} \times \sqrt{A}$ Where:D_S − *Specific elevation difference (m);*I_{pg} − *Overall slope index (m/km);*A − *Total watershed area (km²).*	
Parameters of the watershed hydrographic network		
Order of watercourses *(The order of a watercourse describes the development of a basin's drainage network from upstream to downstream).*	Hierarchy of watercourses according to Strahler	(Strahler A. N., 1957)
The confluence ratio *(This is the ratio between the number of watercourses of order n and the number of watercourses of order n+1)*	$N_C = \frac{N(n)}{N(n+1)}$ Where:N_C − *Confluence ratio of watercourses;*$N(n)$ − *Number of watercourses of order n;*$N(n+1)$ − *Number of watercourses of order "n+1".*	(Schumm S.A., 1956)
The length ratio *(This is the ratio of the average lengths of rivers of order n to the average lengths of rivers of order n-1)*	$N_l = \frac{N(n+1)}{N(n)}$ Where:N_l − *Length ratio of watercourses;*$N(n)$ − *Average length of watercourses of order n (km);*$N(n+1)$ − *Average length of watercourses of the next order "n+1".*	(Horton Robert E., 1945)
Drainage density *(This is the ratio of the total length of permanent and temporary watercourses to the surface area of the watershed).*	$D_d = \frac{\sum_{i=1}^{n} L_i}{A}$ D_d − Drainage density (km/km²); L_i − length of watercourses (km); A − surface area of the watershed.	
Frequency of watercourses or hydrographic density *(This is the ratio of the total number of thalwegs of all orders to the surface area of the watershed).*	$F_C = \frac{\sum N_i}{A}$ Where:F_C − *Frequency of watercourses;*N_i − *Number of watercourses;*A − *Watershed area.*	(Horton R. E., 1932)
Torrentiality coefficient *(This is the product of drainage density and the frequency of elementary watercourses (order 1).)*	$C_t = D_d \times F_{C1} = D_d \times \frac{N_1}{A}$ C_t − *Torrentiality coefficient;*D_d − *Drainage density (km/km²);*F_{C1} − *Frequency of order 1 watercourses;*N_i − *Number of order 1 watercourses;* A − *Watershed area (km²).*	(BRGM & ANTEA, 2014)
Concentration time T_C	$T_C = \frac{0{,}12\sqrt{A}}{\sqrt{P}}$	

ISSN: 1857-7881 (Print)
e-ISSN 1857-7431 (Online)

(This is the time taken for the first raindrop to fall on the furthest point of the basin to reach the outlet).	$T_C = \frac{0{,}1108 \times 3 \times \sqrt{A \times L_t}}{\sqrt{P}}$ *T_C − Concentration time (hours);L_t − Length of the main thalweg (km);P − Weighted average slope in %;A − Watershed area (km²).*	
Flow velocity *(This is the distance traveled by a mass of water per unit of time.)*	$V_e = \frac{L_t}{T_C}$ *V_e − Flow velocity (km/h);L_t − length of the main thalweg (km):T_C − Concentration time (hours).*	(Manning Robert, 1891)

2.3.2. Soil characterization

Step 3: soil characterization is based on data provided by the National laboratory and field measurements (granulometry tests) conducted by the National Agency for Geosciences. This approach enabled the assessment of soil permeability and infiltration capacity (D2487-17, 2025; Robert P. Chapuis, 2003).

2.3.3. Validation of morphometric parameter results

Due to the extent of the study area and financial constraints, we chose to limit morphometric parameter validation to a few watersheds. This strategy will be extended in future studies. For validation, direct field measurements of minimum, maximum, and mean elevation, total thalweg count, and thalweg order were taken. Result accuracy was then calculated as follows:

- calculation of absolute error: $\left|Parameter_{field} - Parameter_{SIG\ or\ EDM}\right|$
- calculation of relative error: $\frac{\left|Parameter_{field} - Parameter_{SIG\ or\ DEM}\right|}{Parameter_{field}} \times 100$

2.3.4. Multivariate statistical analysis method

Step 4: To classify the watershed, its morphometric parameters must first be determined. These parameters are numerous and each has its own unit, leading to a large and complex data matrix that is difficult to interpret. The use of multivariate statistical methods therefore, provides an efficient way of tackling this complexity. The main objective of this analysis is to characterize each watershed using statistical approaches and to assess its morphometric behavior. Researchers such as Faye Cheikh (2014) have already used this strategy to group and interpret the relationships between measured parameters. To this end, two approaches have been adopted to characterize the watershed parameters: Principal Component Analysis (PCA) and Hierarchical Cluster Analysis. PCA is used to reduce the dimensionality of the dataset and to identify the main structural factors controlling the morphology and hydrology of the watersheds. The reduction is only possible if the initial variables are moderately to strongly correlated and not independent (Chirala U, 2012).

ISSN: 1857-7881 (Print)
e-ISSN 1857-7431 (Online)

Many studies, including those by Cloutier & al. (2008), Faye Cheikh (2014), and Faidance Mashauri MM, 2023), have applied this method in hydrological and morphometric analyses.

Data must be carefully prepared before PCA, due to differences in scales and units, the need for standardization, the presence of outliers, and the necessity of checking the correlation between variables. The variable-selection procedure involved removing severe multicollinearity while preserving the representativeness of the tree hydro-morphometric parameters. Given the absence of missing values in the dataset (38 watersheds × 23 variables = 874 complete observations), each variable was transformed into a z-score using the following formula: $Z = \frac{X_{ij} - \underline{X}_j}{\sigma_j}$

Where X_{ij} −is the raw value of basin i for variable j, $\underline{X}_j$ −is the mean of variable j over the 38 basins, et σ_j −the standard deviation.

After this z-score transformation, each variable has a mean of 0 and a standard deviation of 1. Because the variables are expressed in different units, PCA is performed on the Pearson correlation matrix (Pearson, K., 1901). In this case, the Pearson correlation coefficient is calculated as follows:

$$r_{xy} = \frac{cov(x,y)}{\sigma_x \sigma_y} = \frac{\sum_{i=1}^{n} \left(x_i - \underline{x}\right)\left(y_i - \underline{y}\right)}{\sqrt{\sum_{i=1}^{n} \left(x_i - \underline{x}\right)^2 \times \sum_{i=1}^{n} \left(y_i - \underline{y}\right)^2}}$$

Où n −the number of observations, $\underline{x}, \underline{y}$ −are the variables x and de y, $\sigma_x \sigma_y$ −are their respective standard deviations.

Here, our approach follows these steps: (1) data preparation and standardization, (2) computation of the correlation matrix and removal of redundant variables, and (3) assessment of data adequacy (Bartlett's test and KMO) before applying PCA to the retained variables. In this study, the analyzed data include 23 parameters measured on 38 watersheds, grouped into three categories: geometric parameters, relief parameters, and hydrological parameters. Because the variables are expressed in different units, the correlation matrix was used to neutralize scale differences, reveal relationships between variables, and produce the most interpretable and reliable components (Sarita Gajbhiye Meshram, 2017; Stuti Chaudhary, 2021).

One the contribution of each variable to the overall analysis is understood, hierarchical clustering is applied to group the watersheds according to these indicators. Starting with each observation as an individual cluster, this method progressively merges clusters two by two until a single global cluster is formed, producing a hierarchical structure visualized as a dendrogram. Researchers such as Güler et al. (2002), and Faidance Mashauri M. & al. (2023) have used this method to analyze various hydrological and environmental parameters. A set of quantitative indicators was then computed

ISSN: 1857-7881 (Print)
e-ISSN 1857-7431 (Online)

using Python (scikit-learm, scipy, numpy) to classify the watersheds into different groups according to their hydrological potential and capacity to act as water storage units (Gaucherel C., 2003).

Step 5: This step consists of combining the results from Step 3 with those from Step 4. The objective is to assess the water availability potential by combining the results from the multivariate statistical analysis with the soil map.

3. Results

3.1. Determination of morphometric parameters

Hydro-morphometric parameters were automatically extracted using the Arc Hydro extension in ArcGIS, yielding 38 delineated watersheds. Geometric, relief, and hydrographic parameters (talweg order, drainage density, torrentiality coefficient, concentration time, and flow velocity) were either derived from the software or computed manually using empirical formulas (Table 1). Results are presented in Figure 1 and Tables 2, 3, and 4.

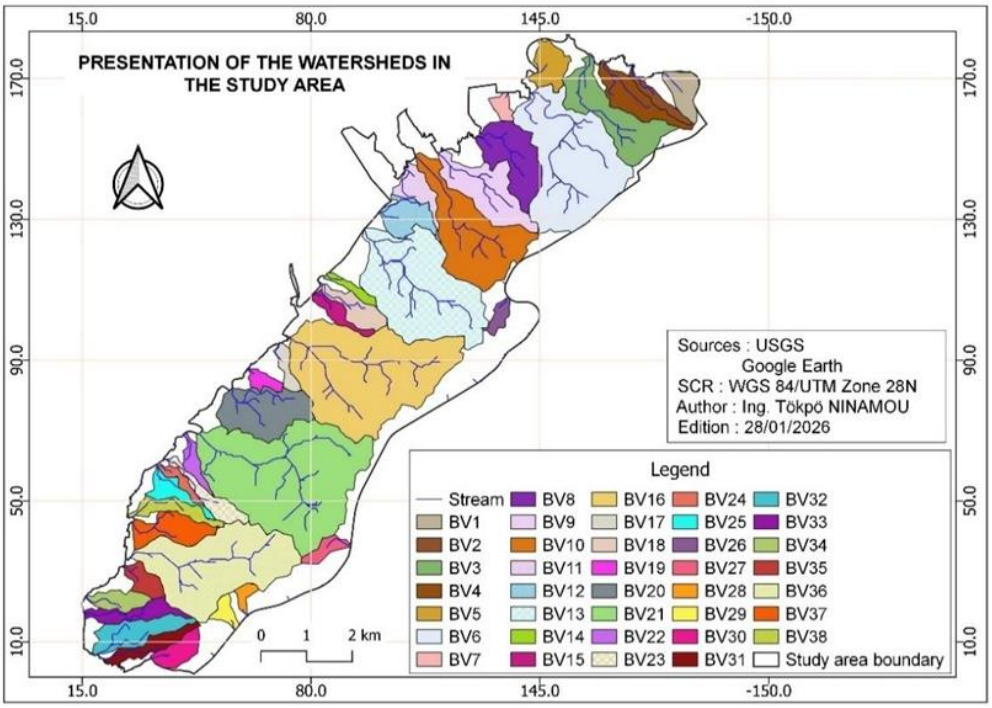

Fig. 1: Presentation of the watersheds in the former municipality of Ratoma

ISSN: 1857-7881 (Print)
e-ISSN 1857-7431 (Online)

Table 2: Hydro-morphometrics characteristics of the watersheds

N° BV	Geometric Parameters								Relief Parameters										Hydrographic Parameters											
	S	P	K_G	L_t	L_{max}	lar_{max}	$L_{éq}$	$lar_{éq}$	D_g	D_s	I_{pg}	Z_{max}	Z_{min}	H_{moy}	$H_{50\%}$	i_{moy}	I_{pm}	I_{pr}	Ord	N_t	L_{t_tal}	R_C	R_l	F	F_1	D_d	C_t	T_C	V_e		
1	0,55	3,29	1,25	0,59	1,31	0,66	1,18	0,46	66,00	41,32	5,59	129,00	58,00	101,06	104,30	0,12	6,01	2,64	1,00	2,00	0,59	0,00	0,00	3,66	3,66	1,08	3,96	0,71	0,74	
2	0,30	4,09	2,10	0,95	1,75	0,22	1,89	0,16	93,80	27,11	4,97	129,00	16,00	83,53	86,50	0,12	5,99	2,49	1,00	1,00	0,95	0,00	0,00	3,36	6,72	2,99	10,04	0,43	1,04	
3	1,92	8,45	1,71	2,81	2,52	1,28	3,71	0,52	93,70	34,98	2,53	121,00	1,00	43,58	27,70	0,03	3,24	1,78	2,00	9,00	4,08	1,25	1,56	4,70	2,61	2,13	5,57	1,87	1,50	
4	0,95	5,88	1,69	1,51	2,46	0,74	2,57	0,37	112,10	42,62	4,37	130,00	3,00	57,28	54,50	0,05	4,95	2,34	3,00	6,00	2,62	2,00	1,42	6,29	3,15	2,75	8,64	1,04	1,44	
5	0,62	3,81	1,36	0,32	1,01	1,20	1,49	0,41	13,80	7,27	0,93	16,00	0,00	6,37	3,00	0,04	1,07	1,08	2,00	4,00	0,44	3,00	1,36	6,47	4,85	0,71	3,46	1,75	0,15	
6	4,86	10,70	1,36	4,16	2,97	2,50	4,19	1,16	84,40	44,42	2,02	99,00	1,00	46,83	41,50	0,01	2,34	1,59	3,00	50,00	10,54	6,67	3,78	10,29	5,56	2,17	12,06	2,78	1,49	
7	0,20	2,02	1,26	0,13	0,62	0,35	0,74	0,27	19,20	11,68	2,60	21,00	0,00	10,72	10,80	0,17	2,85	1,80	1,00	1,00	0,13	0,00	0,00	4,96	4,96	0,22	1,07	0,74	0,14	
8	1,54	6,32	1,42	1,70	2,17	1,19	2,56	0,60	68,10	33,12	2,67	85,00	1,00	26,55	22,00	0,03	3,29	1,83	2,00	11,00	2,44	1,20	0,42	7,12	3,88	1,58	6,14	1,84	0,90	
9	1,67	7,38	1,60	2,14	2,78	1,13	3,16	0,53	82,50	33,67	2,61	91,00	1,00	34,37	25,30	0,03	2,84	1,81	2,00	12,00	3,46	2,00	1,66	7,20	4,80	2,07	9,95	1,81	1,18	
10	3,08	9,78	1,56	3,48	3,35	1,44	4,15	0,74	98,70	41,75	2,38	110,00	0,00	57,10	68,30	0,01	2,65	1,73	3,00	16,00	9,05	3,33	3,87	5,20	3,25	2,94	9,56	2,02	1,71	
11	0,55	4,95	1,86	0,97	1,80	0,81	2,23	0,25	43,50	14,52	1,96	77,00	0,00	10,52	3,80	0,08	3,46	1,56	1,00	1,00	0,97	0,00	0,00	1,81	1,81	1,74	3,15	1,70	0,56	
12	0,74	4,41	1,44	1,05	1,32	0,93	1,80	0,41	39,80	19,01	2,22	63,00	1,00	14,42	10,00	0,05	3,45	1,66	2,00	3,00	1,37	2,00	0,05	4,07	2,72	1,86	5,04	1,70	0,61	
13	4,72	10,43	1,34	3,75	3,59	1,74	4,05	1,17	116,70	62,63	2,88	129,00	0,50	55,59	49,30	0,01	3,18	1,90	3,00	72,00	8,90	5,75	2,96	15,26	9,75	1,89	18,38	2,40	1,55	
14	0,21	2,88	1,75	0,37	1,28	0,20	1,27	0,17	33,60	12,18	2,64	43,00	1,00	21,17	23,30	0,11	3,30	1,82	1,00	1,00	0,37	0,00	0,00	4,71	4,71	1,74	8,18	0,67	0,55	
15	0,35	3,83	1,83	0,60	1,57	0,41	1,71	0,20	47,20	16,19	2,76	68,00	0,50	21,07	20,00	0,11	3,94	1,86	1,00	1,00	0,60	0,00	0,00	2,90	2,90	1,73	5,01	0,89	0,66	
16	6,26	11,83	1,32	3,67	3,38	2,44	4,53	1,38	98,90	54,60	2,18	128,00	1,50	58,20	58,10	0,01	2,79	1,65	3,00	26,00	16,88	3,33	1,55	4,15	2,08	2,69	5,59	2,57	1,42	
17	0,27	2,81	1,51	0,49	1,14	0,33	1,18	0,23	24,70	10,96	2,10	30,00	1,50	19,43	21,60	0,06	2,42	1,62	1,00	1,00	0,49	0,00	0,00	3,67	3,67	1,74	6,38	0,83	0,57	
18	0,61	4,04	1,45	1,40	1,73	0,60	1,65	0,37	58,80	27,80	3,57	70,00	0,00	31,38	28,60	0,05	4,24	2,11	2,00	3,00	1,32	2,00	2,12	4,93	3,29	2,17	7,15	1,12	1,13	
19	0,22	2,38	1,41	0,17	0,88	0,39	0,96	0,23	18,10	8,96	1,89	27,00	3,00	16,34	17,90	0,14	2,51	1,54	1,00	1,00	0,17	0,00	0,00	4,45	4,45	0,77	3,41	0,74	0,23	
20	1,76	6,18	1,30	1,94	1,92	1,09	2,33	0,76	56,40	32,08	2,42	70,00	1,00	25,05	22,20	0,00	2,96	1,74	5,00	556,00	25,62	4,50	1,43	315,50	173,64	14,54	2524,26	2,09	0,92	
21	7,00	12,72	1,35	4,05	3,71	2,61	4,94	1,42	92,40	49,46	1,87	127,00	2,00	60,05	62,40	0,01	2,53	1,53	3,00	78,00	12,71	2,50	1,03	11,14	5,71	1,81	10,37	2,73	1,47	
22	0,29	3,39	1,75	0,84	1,51	0,38	1,50	0,20	43,70	15,79	2,91	63,00	2,00	22,19	20,00	0,07	4,06	1,91	1,00	1,00	0,84	0,00	0,00	3,40	3,40	2,87	9,73	0,87	0,74	
23	0,56	5,29	1,98	1,74	2,31	0,51	2,41	0,23	77,70	24,11	3,22	96,00	1,00	59,67	65,70	0,05	3,94	2,01	1,00	1,00	1,74	0,00	0,00	1,78	1,78	3,05	5,44	0,91	1,88	
24	0,22	3,15	1,90	0,33	1,32	0,33	1,42	0,15	49,00	15,98	3,44	60,80	1,00	25,98	23,00	0,18	4,20	2,07	1,00	1,00	0,33	0,00	0,00	4,63	4,63	1,38	6,39	0,58	0,52	
25	0,43	4,62	1,98	0,76	1,76	0,83	2,11	0,20	59,10	18,37	2,81	82,50	1,00	28,20	23,70	0,11	3,87	1,87	1,00	1,00	0,76	0,00	0,00	2,33	2,33	1,76	4,10	0,90	0,84	
26	0,23	2,47	1,45	0,33	0,91	0,36	1,01	0,23	25,80	12,21	2,56	127,00	89,00	115,50	117,00	0,05	3,77	1,79	1,00	1,00	0,70	0,00	0,00	4,40	4,40	3,09	13,57	0,58	0,56	
27	0,29	2,75	1,42	0,65	1,12	0,35	1,11	0,26	24,00	11,72	2,16	127,00	89,00	112,74	113,30	0,06	3,42	1,64	1,00	1,00	0,65	0,00	0,00	3,40	3,40	2,21	7,49	0,81	0,80	
28	0,16	2,09	1,44	0,20	0,71	0,38	0,85	0,19	18,60	8,84	2,19	103,00	79,00	93,87	94,60	0,12	2,82	1,65	1,00	1,00	0,20	0,00	0,00	6,11	6,11	1,21	7,36	0,61	0,29	
29	0,23	2,34	1,37	0,25	0,73	0,69	0,92	0,25	28,50	14,87	3,10	110,00	75,00	95,13	95,80	0,14	3,81	1,97	1,00	1,00	0,25	0,00	0,00	4,35	4,35	1,07	4,67	0,63	0,38	
30	0,48	3,10	1,25	0,42	1,19	0,48	1,12	0,43	49,00	30,44	4,38	111,00	30,00	61,46	59,20	0,07	7,24	2,34	2,00	18,00	1,12	17,00	4,96	37,30	35,22	2,32	81,87	0,76	0,56	
31	0,52	5,06	1,96	1,87	2,18	0,41	2,30	0,23	82,80	26,05	3,60	114,00	3,00	42,09	41,90	0,06	4,82	2,12	1,00	1,00	1,87	0,00	0,00	1,91	1,91	3,56	6,78	1,14	1,64	
32	0,95	5,61	1,61	1,44	2,35	0,71	2,41	0,40	67,90	27,49	2,82	110,00	-2,00	34,30	27,60	0,05	4,65	1,88	2,00	4,00	2,25	3,00	0,16	4,20	3,15	2,36	7,43	1,25	1,12	
33	0,59	5,53	2,01	1,73	2,33	0,50	2,53	0,24	57,70	17,59	2,28	99,00	3,00	36,53	32,80	0,06	3,79	1,69	1,00	1,00	1,73	0,00	0,00	1,68	1,68	2,91	4,89	1,22	1,41	
34	0,46	3,36	1,39	0,99	1,42	0,51	1,34	0,34	30,20	15,21	2,25	52,30	-1,00	24,28	20,60	0,05	3,98	1,68	1,00	1,00	0,99	0,00	0,00	2,19	2,19	2,17	4,77	1,01	0,90	
35	0,40	2,91	1,28	0,44	1,11	0,63	1,08	0,37	45,30	26,67	4,20	57,00	1,00	33,87	35,90	0,09	5,19	2,29	2,00	3,00	0,61	2,00	0,73	7,43	4,95	1,51	7,47	0,70	0,62	
36	4,38	10,24	1,37	3,77	3,81	2,06	4,03	1,09	107,70	55,86	2,67	129,00	0,00	70,18	76,00	0,02	3,20	1,83	3,00	43,00	7,35	1,00	1,45	9,82	5,71	1,68	9,57	2,09	1,80	
37	0,89	5,02	1,49	1,21	1,88	0,78	2,08	0,43	72,70	33,02	3,49	88,00	-1,00	38,94	35,40	0,05	4,27	2,09	2,00	3,00	1,87	2,00	1,01	3,35	2,24	2,09	4,67	1,13	1,14	
38	0,52	5,08	1,97	1,52	2,11	0,47	2,32	0,22	73,90	23,00	3,19	89,00	1,00	37,53	30,00	0,06	3,80	2,00	1,00	1,00	1,52	0,00	0,00	1,92	1,92	2,89	5,55	1,06	1,41	

S – watershed area; P – watershed perimeter; KG – Gravelius compactness coefficient or index; Lt – total length of main thalweg; Leq – length of equivalent rectangle; $léq$ - – width of equivalent rectangle; Lmax – maximum length; $lmax$ – maximum width; Dg - overall elevation difference; Ds - specific elevation difference; I pg - overall slope index (%); Z max– maximum altitude; Z min – minimum altitude; H moy. – average altitude; I pm – Average Slope Index; I pr– Rock Slope Index; Order - order of the thalweg; Nt - Total number of thalwegs; Lcp - Length of the main watercourse; Lt -total length of thalwegs; RC - Confluence ratio; Rl - Average length ratio; F - Hydrographic density; D(d) - Drainage density; C(t) - Torrentiality coefficient; T(C) - Concentration time; V(e) - Water flow velocity

ISSN: 1857-7881 (Print)
e-ISSN 1857-7431 (Online)

The analysis of Table 4 shows that 16.67% of the basins exhibit very low flow velocities (< 0.5 m/s), 36.67% low velocities (0.5-0.8 m/s), and 46.66% moderate velocities (0.8-2.5 m/s). In contrast, all basins in Group 2 display flow velocities within the 0.8-2.5 m/s range.

3.2. Soil mapping

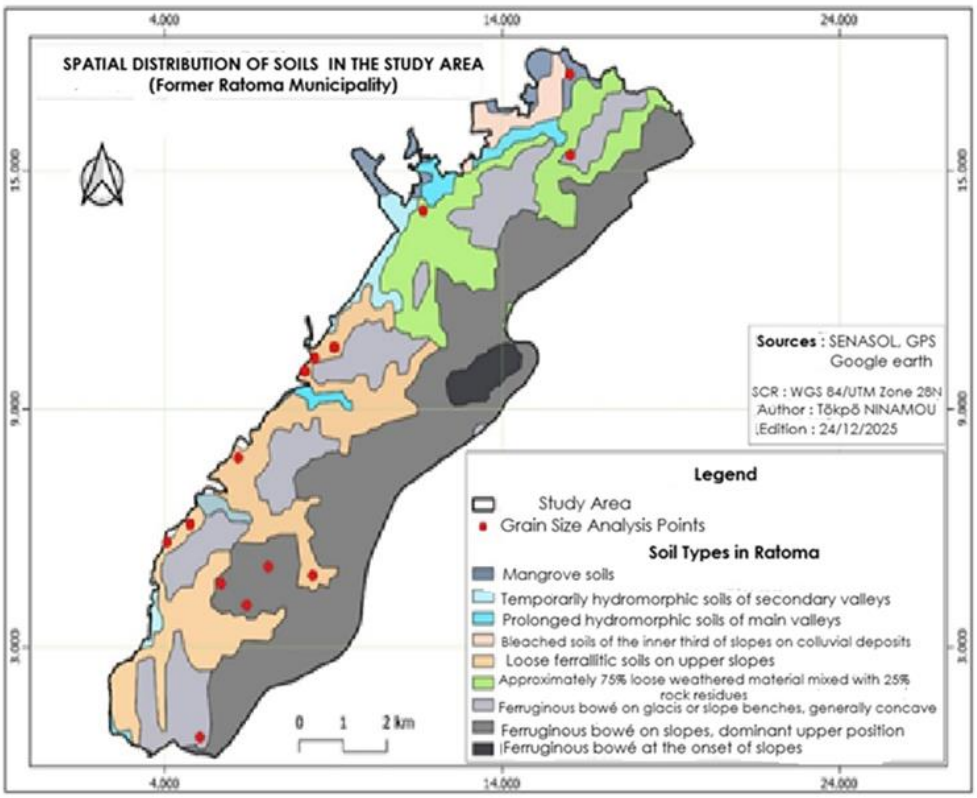

Fig. 2: Soil map of Ratoma

The pedological inventory based on Figure 2 allowed the identification of nine main units, distributed as follows:

- Dominant units (+15% of the area): Ferruginous upper slope bowé (38.25%), loose ferrallitic soils (18.95%) and glacis bowé (18.38%);
- Secondary units (5-15% of the area): Mixture of weathered rock (12.65%)
- Minor units (<5% of the area): Mangrove soils (2.98%), prolonged hydromorphic soils (2.37%), temporary hydromorphic soils (2.24%).
- Decolorized soils (2.23%), and slope-initiating bowé (1.95%).

ISSN: 1857-7881 (Print)
e-ISSN 1857-7431 (Online)

To confirm this distribution (Fig. 2), we used granulometric analysis results (Table 5) from the Conakry Geosciences Agency on the foundation-study sample collected within the study area for this research.

Table 3: Granulometric and qualitative analysis of soil samples

Sample	Depth (m)	% retained Ø ≥ 2 mm	% passing Ø < 2 mm	Qualitative interpretation			
				Dominant texture	Infiltration tendency	Water reserve	Probable apparent texture
EHamCon	3 à 5,6	58.7	41.3	Squelettique	Élevée	Très faible	Sableux grossier à gravillonneux
Ekaporo	4 à 6	19.3	80.70	Modérément grossier	Modérée	Moyenne à faible	Sable-limoneux gravillonneux
Ekipé1	1,5 à 3	19.7	80.3	Peu grossier	Moyenne à faible	Bonne	Limono-sableux ou limono-argileux
Ekipé2	1,5 à 3	73.5	26.5	Très grossier	Élevée	Très faible	Sable grossier / bowé caillouteux
Ekipé3	3 à 5	60.4	39.6	Très grossier	Élevée	Très faible	Sable ferrallitique ou régosol
Ekoloma	4 à 6	38.9	61.1	Modérément grossier	Modérée	Moyenne	Sable-limoneux ou ferrallitique meuble
Esonfon	6 à 7	18.9	81.1	Peu grossier	Faible à modérée	Bonne	Limono-argileux décoloré
Ekipé4	4 à 6	15.2	84.8	Peu grossier	Faible	Élevée	Argilo-limoneux ou hydromorphe temporaire
Ekipé5	3,5 à 5	55.8	44.2	Très grossier	Élevée	Faible	Sableux à caillouteux (glacis ferrugineux)
ENongTa1	3 à 4	37.8	62.2	Modérément grossier	Modérée	Moyenne	Sable-limoneux à ferrallitique
ENongTa2	1,5 à 3	43.6	56.4	Modérément grossier	Modérée	Moyenne à faible	Sable-limoneux
Esonforad	2,5 à 4	52.6	47.4	Très grossier	Élevée	Faible	Sable gravillonneux à ferrugineux
Ekobaya	5 à 7	34.2	65.8	Modérément grossier	Modérée	Moyenne	Sable-limoneux à tendance argileuse
Elamba	4 à 5	22.60	77.40	Modérément grossier	Modérée	Moyenne	Sable-limoneux gravillonneux

Results in Table 3 allow classification of soils based on the proportion of coarse elements retained on a 2mm sieve. Analysis shows that five samples (EHamCon, Ekipé2, Ekipé3, Ekipé5, and Esonforad) have skeletal textures,

ISSN: 1857-7881 (Print)
e-ISSN 1857-7431 (Online)

confirming their mapped locations (Fig. 2). A qualitative approach was used to estimate infiltration potential by combining soil map interpretation with granulometric data. Samples containing at least 50% coarse fragments (≥2 mm) are likely well drained, with high infiltration capacity but very low water retention. In contrast, soils with low coarse content (Ekipé1, Esonfon, Ekipé4) show infiltration dependent on fine texture and may exhibit temporary hydromorphic conditions.

3.3. Validation of morphometric parameter results

Table 4: Validation of morphometric parameters

Paramètre	Bassin versant	Valeur (m)		Erreur		Précision du MNT par rapport à la mesure terrain
		Pris sur terrain	SIG	Absolue	Relative (%)	
Altitude minimale	BV1	57,85	58	0,15	0,26	Very reliable
Altitude maximale	BV6	99,17	99	0,17	0,17	Very reliable
Altitude moyenne	BV20	26,88	25,05	1,83	6,81	Reliable
Pente moyenne	BV28	0,142	0,12	0,02	15,49	Moderately reliable
Altitude maximale	BV3	112,25	121	8,75	7,80	Reliable
Pente moyenne	BV19	0,19	0,14	0,05	26,32	Moderately
Ordre du talweg	BV32	2	2	0	0,00	Very reliable
Nombre total de Talweg	BV26	1	1	0	0,00	Very reliable
Ordre du talweg	BV25	4	5	1	25,0	Moderately

The results indicate a good agreement between the morphometric parameters derived from the DEM and the field measurements, particularly for minimum, maximum and mean elevation, whose relative errors are generally below 10%. Larger discrepancies observed for mean slopes and for the order of certain thalwegs reflect both the limitation of the DEM and the sensitivity of these parameters to the measurement methods.

3.4. Multivariate statistical analysis

Principal Component Analysis is used to highlight affinities between different watersheds and understand the dependence among morphometric parameters, in order to identify the main axes of morphometric variability.

Variables show very different orders of magnitude (for example, S in km² with a CV of 134,7% compared to KG without dimension with a CV of 16,4%). The Shapiro-Wilk test indicates that 3/23 variables are normally distributed, and standardization combined with PCA robustness compensates for this asymmetry. The correlation matrix (38×23) of the initial parameters reveals many strong correlations, including several pairs with $|\boldsymbol{r}| > \mathbf{0,90}$, indicating high redundancy among some variables. Matrix analysis identified 17 pairs with $|\boldsymbol{r}| > \mathbf{0,90}$, grouped as follows:

ISSN: 1857-7881 (Print)
e-ISSN 1857-7431 (Online)

- Geometric parameters: S – P (0,94), S – Lt (0,91), S – lmax (0,95), S – Tc (0,96), P – Lt (0,98), P – Lmax (0,95), P – Léq (0,99), Lt – Léq (0,97), lmax – Tc (0,92);
- Relief parameters: Ipg – Ipr (0,99), Hmoy – H50% (0,99) ;
- Hydrographic parameters: F – F1 (0,99), F – Ct (0,99), F – Dd (0,93), F1 – Ct (0,99), Dd – Ct (0,94).

In total, 10 variables were removed: S, P, Léq, L_{talw}, $H_{moy.}$, Ipg, F, F1, Dd, Tc. The remaining 13 variables are: KG, Lmax, lmax, Ds, H50%, Imoy., Ipm, Ipr, Rc, Rl, Ct, Ve.

Table 5: Correlation matrix of 13 selected variables after redundancy removal

	KG	Lmax	lmax	Ds	H50%	Imoy	Ipm	Ipr	Lt_hydro	Rc	Rl	Ct	Ve
KG	1												
Lmax	0,07	1											
lmax	-0,38	0,79	1										
Ds	-0,26	0,86	0,77	1									
H50%	-0,18	0,03	0,03	0,21	1								
Imoy	0,01	-0,56	-0,47	-0,45	-0,11	1							
Ipm	0,2	-0,18	-0,43	0,07	0,28	0,1	1						
Ipr	0,18	-0,07	-0,34	0,24	0,33	0,17	0,89	1					
Lt_hyd	-0,31	0,6	0,7	0,62	0,02	-0,42	-0,31	-0,22	1				
Rc	-0,41	0,21	0,33	0,4	0	-0,26	0,26	0,1	0,33	1			
Rl	-0,39	0,47	0,54	0,6	0,05	-0,37	0,02	0,02	0,44	0,85	1		
Ct	-0,18	0	0,06	0,07	-0,11	-0,15	-0,09	-0,06	0,69	0,18	0,1	1	
Ve	0,26	0,87	0,51	0,73	0,16	-0,56	0,04	0,16	0,44	0,09	0,35	-0,01	1

Two statistical tests, reported in Table 6, were applied to validate the dataset for factor analysis: Bartlett's sphericity test, with the null hypothesis of an identity matrix, and the Kaiser-Meyer-Olkin (KMO) measure of sampling adequacy.

Table 6: Validation of data adequacy

Dataset	Bartlet's test (p-value)	Overall KMO index
23 initial variables	≈ 0	0,808
13 final variables	≈ 0	0,8098

After analyzing the correlation matrix, three principal axes were retained (Table 7) based on cumulative variance exceeding 70%, explaining 72,92% of the total variance in the morphometric dataset.

Table 7: Eigenvalues of the correlation matrix of morphometric parameters

Component	Eigenvalue λ (%)	% variance	% Cumulative	Retained (≥ 70%)
CP1	5,18	39,86	39,86	Oui
CP2	2,44	18,79	58,86	Oui
CP3	1,86	14,28	72,92	Oui
CP4	1,23	9,46	82,38	Oui
CP5	1,05	8,09	90,46	Oui
CP6	0,52	4,03	94,49	Non

ISSN: 1857-7881 (Print)
e-ISSN 1857-7431 (Online)

CP7	0,34	2,63	97,13	Non
CP8	0,18	1,38	98,51	Non
CP9	0,07	0,54	99,04	Non
CP10	0,05	0,39	99,43	Non
CP11	0,03	0,27	99,70	Non
CP12	0,03	0,24	99,94	Non
CP13	0,01	0,06	100,00	Non

The factor structure of the morphometric dataset is well captured by three principal axes, summarizing 72,92% of the total information, which is statistically satisfactory for an initial 13-dimensional space.

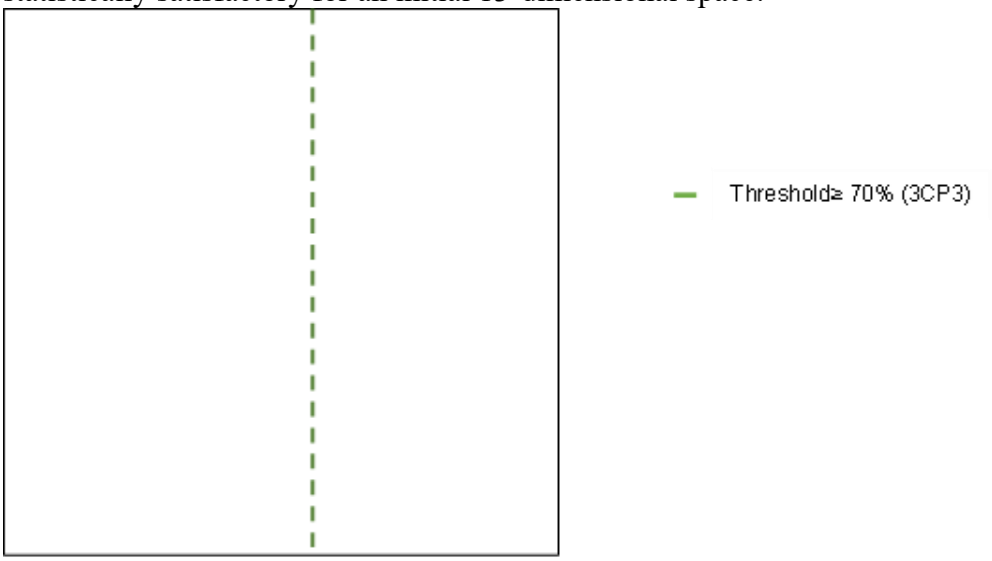

Figure 3: Scree plot of eigenvalues with indication of the Kaiser threshold and cumulative variance.

To define the weights of each variable in constructing the components, Table 8 was prepared.

Table 8: Eigenvalues (weighting coefficients) for PC1, PC2, and PC3

Variable	CP1	CP2	CP3
KG	2,087	1,461	**27,546**
Lmax	**14,437**	0,464	**10,953**
larmax	**15,036**	1,671	0,258
Ds	**14,603**	5,269	0,523
H50%	0,104	**9,093**	0,139
Imoy	**13,442**	0,852	0,798
Ipm	1,151	**33,211**	1,398
Ipr	0,511	**34,745**	0,125
Lt_tal	**12,622**	1,830	0,919
RC	5,148	3,130	**22,883**
Rl	**10,012**	1,840	**9,649**
Ct	1,354	2,114	7,407
Ve	**9,492**	4,319	**17,403**

ISSN: 1857-7881 (Print)
e-ISSN 1857-7431 (Online)

Dominant variables are shown in bold for each component. They correspond to the highest contributions along each axis.

PC1 is dominated by Lmax (14,437), lmax (15,036), imoy (13,442), Ds (14,603), Lt_tal (12,622). It is composed of variables reflecting attributes directly related to basin spatial extent and drainage network density. PC1 explains 39,86% of the total variance and represents the dimensional morphometric axis. PC2 accounts for 18,79% of the total variance and reflects relief characteristics. Ipr (34,75) and Ipm (33,21) are indicators of slope steepness, while H50% (9,09) reflects the general altitudinal position of the basin. PC3 is mainly structured by KG (27,55), Rc 22,88), Ve (17,40), Lmax (10,95) et Rl (9,65).

Table 9: Eigenvalues of correlation matrix (weighting coefficients)

N°	Individuals	CP1	CP2	CP3	N°	Individuals	CP1	CP2	CP3
1	**BV1**	0,803	11,871	1,301	**20**	**BV20**	6,51	5,69	12,11
2	**BV2**	1,947	11,337	1,913	**21**	**BV21**	9,41	1,25	1,11
3	**BV3**	1,217	0,037	1,892	**22**	**BV22**	1,34	0,03	0,35
4	**BV4**	0,384	5,946	0,595	**23**	**BV23**	0,01	1,36	7,33
5	**BV5**	0,093	17,569	2,367	**24**	**BV24**	4,33	0,24	0,13
6	**BV6**	10,919	0,638	0,599	**25**	**BV25**	1,15	0,01	1,85
7	**BV7**	4,342	2,397	2,840	**26**	**BV26**	1,38	0,00	0,47
8	**BV8**	0,184	0,430	0,055	**27**	**BV27**	0,96	0,13	0,12
9	**BV9**	1,113	0,221	0,581	**28**	**BV28**	3,06	1,02	1,10
10	**BV10**	7,039	0,034	0,278	**29**	**BV29**	2,76	0,07	1,69
11	**BV11**	0,965	2,160	0,972	**30**	**BV30**	0,56	17,70	37,33
12	**BV12**	0,238	1,790	0,292	**31**	**BV31**	0,14	2,43	5,02
13	**BV13**	9,819	0,640	0,027	**32**	**BV32**	0,00	0,31	0,21
14	**BV14**	2,721	0,567	0,070	**33**	**BV33**	0,17	0,04	5,62
15	**BV15**	2,004	0,061	0,435	**34**	**BV34**	0,59	0,78	0,01
16	**BV16**	10,751	0,515	0,137	**35**	**BV35**	0,72	2,06	2,65
17	**BV17**	1,306	3,723	0,008	**36**	**BV36**	7,46	0,24	2,52
18	**BV18**	0,012	0,875	0,346	**37**	**BV37**	0,04	0,83	0,00
19	**BV19**	3,333	4,776	0,984	**38**	**BV38**	0,21	0,23	4,71

Basins with the highest PC1 scores are BV6, BV16, BV13, V21, BV36 and BV10. These basins are characterized by large planar dimensions, high drainage density, and long total stream length. The correspond to hydrological units likely to generate high runoff discharge. Those with high PC2 scores are BV30, BV5, BV1 and BV2. Thes basins are characterized by steep slopes and high H50% values. They present a higher hydrological risk in terms of flash floods, sediment transport, and slope erosion. Finally, the highest PC3 scores concern BV30, BV20, BV23, BV33 and BV31. These basins are either elongated (KG >> 1) or highly irregular in shape. Only BV30 shows high scores on both PC2 (17,70) and PC3 (37,33), making it both a high-relief basin and a strongly atypical morphometric form. Basins with low scores on all three axes are BV8, BV22, BV27, BV32 and BV34. They represent basins with

ISSN: 1857-7881 (Print)
e-ISSN 1857-7431 (Online)

moderate size, relief, and morphometric complexity. Overall, the PCA highlights clear functional and morphological contrasts among the studied basins, linking form, relief, and hydrological response patterns in watersheds.

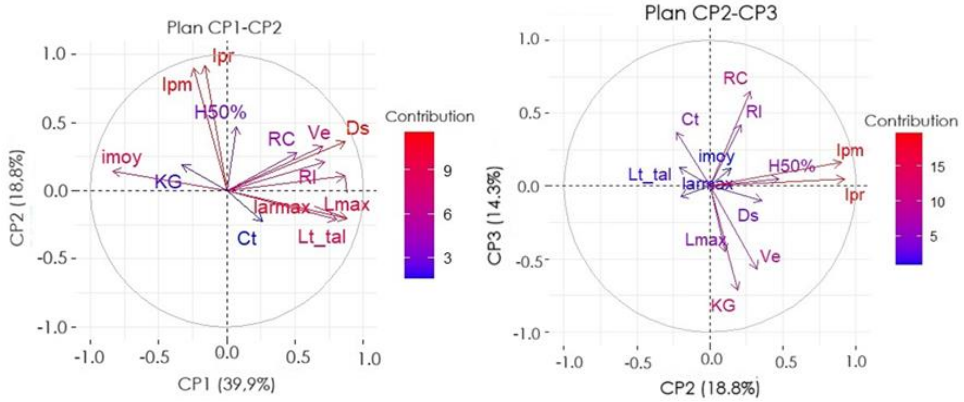

Figure 4: Correlation circles in the PC1-PC2 and PC2-PC3 planes

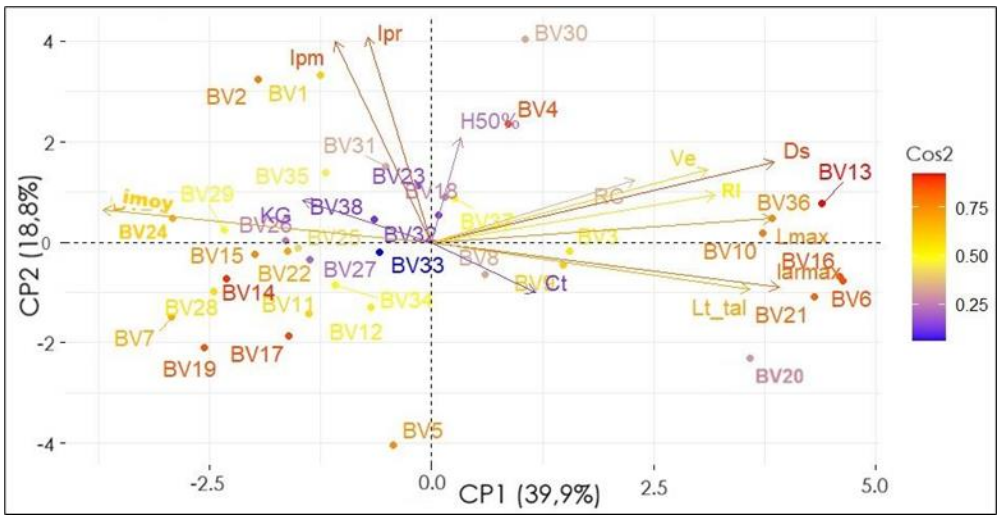

Figure 5: Biplot of individuals and variables in the PC1-PC2

To understand the hierarchical relationships among the 38 watersheds, agglomerative hierarchical clustering was applied using Ward's method as the linkage criterion. The resulting dendrogram (Fig. 6) illustrates the clustering structure and allows visualization of how the groups are formed.

ISSN: 1857-7881 (Print)
e-ISSN 1857-7431 (Online)

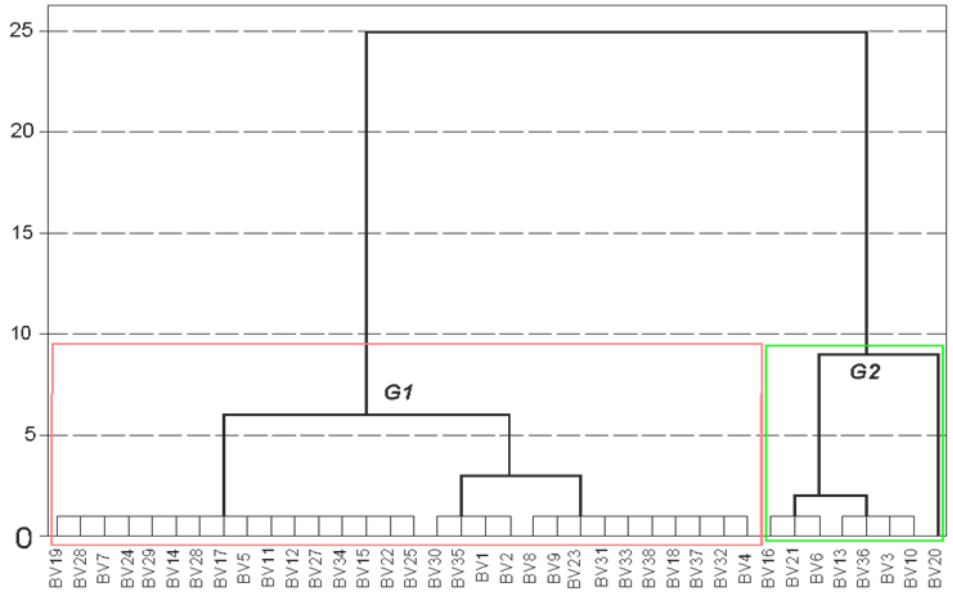

Figure 6: Dendrogram of agglomerative hierarchical clustering of the watersheds

The dendrogram shows a clear two-group partition contrasting hydro-morphometric characteristics: Groupe 1 (30 BV), and Groupe 2 (7 BV).

The map below spatially represents the results of the hierarchical clustering analysis within the study area.

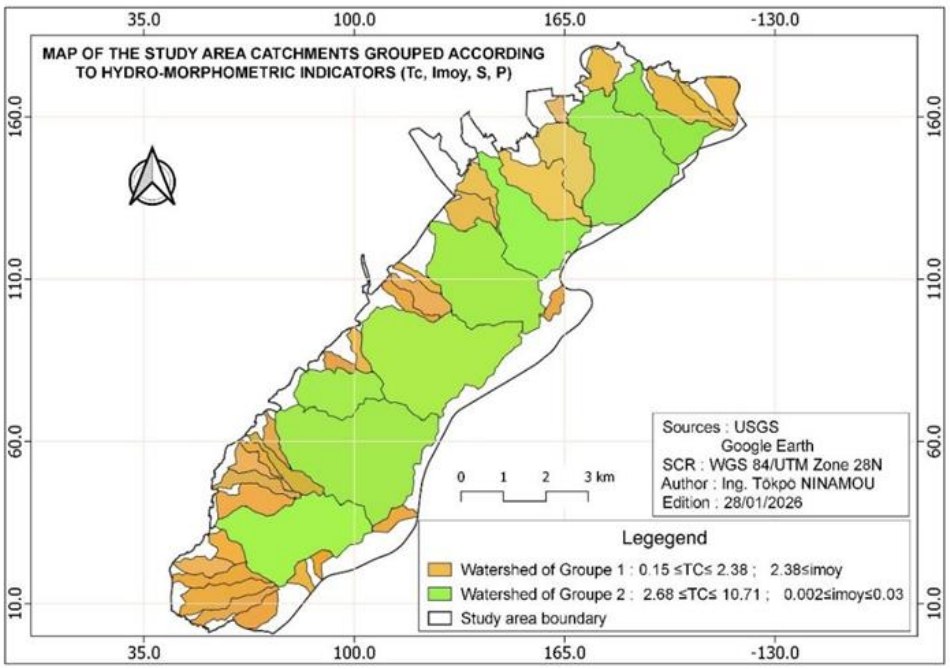

Figure 7: Ratoma map showing the grouping of the 38 watersheds based on morphometric indicators

ISSN: 1857-7881 (Print)
e-ISSN 1857-7431 (Online)

3.5. Assessment of the water availability potential of the watersheds in the study area

This section addresses the assessment of water availability potential in drainage basins by integrating several factors, including concentration time, flow velocity, pedology, and soil texture (encompassing permeability and water retention), based on a multivariate analysis:

The upstream sub-basins have steep slopes and low drainage density, resulting in high concentration time. Deep soils, rich in organic matter and without a crust, can act as reservoirs for retention and infiltration, while very skeletal soils and bogs are less favorable. Samples containing a high proportion of coarse particles (>50%) have high gravitational conductivity but low storage capacity. However, samples with a high silt or clay content have low hydraulic conductivity (Ks) but high surface retention. Principal component analysis highlights three sensitivity axes, while hierarchical clustering distinguishes two watershed groups with different soil textures affecting water retention and storage capacity characteristics.

Based on this analysis, two functional classes were identified: (i) infiltration areas with high potential, and (ii) transit areas with moderate particle transport.

4. Discussion

4.1. Analysis of morphometric parameters of the Ratoma watersheds

The results in Table 7 show that, for some basins, the structure of the drainage network is well reproduced, with identical thalweg order and count. Despite its limitations, the DEM used can therefore be considered sufficiently reliable for the overall morphometric characterization of the studied basins.

Tables 2 and 5 reveal strong dimensional variability among the watersheds, with areas ranging from 0,164km² to 7km² and perimeters varying from approximately 2,022 to 12,72m. This diversity reflects the coexistence of very small, localized basins alongside larger basins capable of generating more complex flow processes, as confirmed by Víg et al. (2022). The KG coefficient varies from 1,245 to more than 2,099, indicating that several basins significantly deviate from a circular shape. More compact basins generally respond more quickly to rainfall events, while elongated basins promote a more gradual temporal distribution of runoff. This observation is consistent with the findings of Boothroyd et al. (2023).

Geometric parameters analysis also shows that nearly 11% of the watersheds (BV1, BV7, BV30, and BV35) have a Gravelius compactness coefficient tending toward 1, reflecting a circular shape conducive to more efficient drainage. These results corroborate the observations of Benzougagh (2019) and Ameur N. (2020), who demonstrated the influence of geometry on the hydrological behavior of basins. Topographic parameters indicate

ISSN: 1857-7881 (Print)
e-ISSN 1857-7431 (Online)

significant contrasts between gently sloping basins and basins with higher relief energy, with Dg values that can exceed 100 m and locally high imoy values. These differences reflect spatial variability in potential energy available for runoff and erosion. Busico et al. (2020) highlighted the central role of urban topography in the runoff process. Hydrological results show contrasting drainage network organization, from first-order basins with a single thalweg to highly developed systems such as BV20, which reaches order 5 and includes 556 thalwegs. This hierarchy reflects major differences in drainage structure (Le Xuan Kham, 2008). The torrentiality coefficient also shows extreme values, with BV20 reaching 2524,26, indicating a highly structured and energetic basin. The concentration time ranges from 0,08 hours to over 10 hours, while the flow velocity ranges from 0,14 to 1,88 m/s. These results confirm that some basins respond rapidly to rainfall, while others respond more slowly. Studies by Echeverri-Díaz et al. (2022) confirm this analysis.

These various results show that the hydrological behavior of the Ratoma watersheds does not depend on a single parameter, but rather on the combination of watershed geometry, relief energy, and drainage network density. The analysis of 13 watersheds in Bangladesh conducted by Alam & al. (2021) confirms this analysis.

4.2. Statistical analysis of the morphometric parameters of the Ratoma watersheds

To better understand the relationship among variables, the correlation coefficient matrix was used to identify links between morphometric parameters. This technique has been used by Baba-Hamed K. (2016) and Faye Cheikh (2014). Accordingly, Table 5 presents the correlation matrix of the 13 selected morphometric parameters, serving as a preliminary step to PCA.

The PCA applied to the dataset produced robust results. The Kaiser-Meyer-Olkin index reached 0.8098, indicating good sampling adequacy according to Gilbert Saporta (2003). PCA reduced the dimensionality to three principal axes, which summarize the information and explain 72.92% of the total variance (Table 7 and Fig. 2). The selection of these three components (Tables 7, 8, and 9) is considered appropriate, consistent with (Henson et al., 2001).

Axis 1 has an eigenvalue of 5,18 and explains 39,86% of the variance. It shows strong positive correlation among Ds, imoy, Lt_tal, Lmax, RI, Ve, larmax and (Table 7 and Fig. 2). These variables describe basin size and drainage characteristics, reflecting spatial extent and hydrographic networks intensity. Basins strongly associated with this axis have large areas, long drainage networks, and well-developed morphology. Axis 2 has an eigenvalue of 2,44 and explain 18,79% of the variance. This axis also indicates a strong

ISSN: 1857-7881 (Print)
e-ISSN 1857-7431 (Online)

positive correlation among the variables (Ipm, Ipr, H50%), indicating topographic and energetic-related characteristics. Axis 3, with an eigenvalue of 1,86, explains 14,25% of the variance and shows strong correlations among Lmax, KG, RC, Rl. These variables describe basin compactness and shape, which influence concentration time. This structure is consistent with studies West African watershed morphometry (Kouassi, 2010)

In Figure 5, the right quadrant (CP1 > 0) contains large, well-drained basins such as BV6, BV13, BV16, BV10, BV36, BV21, BV3, and BV20. The upper quadrant (CP2 > 0) contains basins with pronounced topography, notably BV30, BV1, and BV2. BV30 appears as a morphometrically exceptional basin, combining steep slopes and significant size. The left quadrant (CP1 < 0) contains smaller basins with steep slopes and low drainage density, including BV7, BV19, BV17, BV24, BV29, BV14, and BV28. Basins BV8, BV22, BV27, and BV32 are near the origin, indicating average morphometry characteristics. BV33 stands out due to a very low cos^2, indicating that it is poorly represented in the CP1-CP2 plane and that its information is carried by CP3. The work of Dahiphale et al. (2024), López-Pérez & Fernández-Reynoso (2021), and shows that large, well-drained basins often project onto an axis related to size, drainage density, and stream frequency.

Group 1 (Figure 6) is characterized by CP1 scores centered on negative values and moderate to high CP2 scores. These basins have a short concentration time (Tc < 1.87 h) and a high average slope (avg. > 0.03). This classifies them as basins with potentially torrential behavior. The dendrogram shows smaller fusion distances (5 to 6), indicating residual heterogeneity within this group. Group 2, on the other hand, is distinguished by strongly positive CP1 coordinates. It comprises the largest and best-drained basins. Values of Tc ≥ 1,87h and Imoy between 0.002 and 0.03 indicate a slower and better-regulated hydrological response, corresponding to basins with large catchment areas and well-developed drainage networks. Figure 7 reveals that the G1/G2 dichotomy is not spatially random. This spatial organization is typical of the crystalline reliefs of West Africa, where differential erosion has progressively concentrated the hydrographic network along zones of geological weakness (Coulibaly Léréyaha et al., 2025).

The results of the PCA and CAH are highly consistent with one another, confirming their reliability. The basins classified as G2 by the CAH (BV6, BV13, BV10, BV36, BV21, BV3, BV20) are exactly the same as those with the highest CP1 scores in the biplot.

4.3. Pedological analysis of the watersheds in the study area

Combining soil with morphometric analysis provides a comprehensive assessment of water availability in watersheds, because morphometry controls

ISSN: 1857-7881 (Print)
e-ISSN 1857-7431 (Online)

surface runoff and infiltration, while soil properties govern subsurface storage and water retention. The nine soil types shown in Figure 3 are grouped into three main trends. The first is the dominance of ferruginous and ferrallitic formation on plateaus and slopes, as confirmed by Faure Paul (1998). The second trend includes a mixture of weathered materials and rock fragments (12,65%), indicating transitional morpho-pedological zones. The third group consists of hydromorphic and decolorized soils (<5%), located in lower slopes and valley bottoms, indicating temporary or permanent water saturation dynamics. These observations agree with Hector Basile (2018) on lowland saturation processes.

Samples collected by the Geoscience Agency of Conakry in Ratoma confirm this spatial distribution. Granulometric analysis results (Table 3) show strong textural heterogeneity, with coarse element content (≥ 2 mm) ranging from 0 to more than 70%. Studies by Adebisi N. (2014), Diop Baye Oumar (2018), and Dzoualou Sorel Dzaba (2024), and also support this interpretation.

The combined interpretation of granulometric data and the soil map (Figure 2) allowed the proposal of a qualitative textural classification and evaluation of infiltration potential for the soil types listed in Table 3. Samples with coarse particle content exceeding 50% (EHamCon, Ekipé2, Ekipé3, Ekipé5, Esonforad) are classified as skeletal or gravelly soils. These soils are generally well drained and show high infiltration capacity but low water retention. Steffen Beck-Broichsitter (2023) demonstrates that gravel content strongly influences pore distribution, water retention capacity, and infiltration behavior. These properties are typical of ferruginous bowé soils and glacis formations, where sandy matrices dominate and fine horizons are poorly developed (Kadéba Abel, 2020). In contrast, fine-textured or moderately coarse sample (Ekipé1, Esonfon, Ekipé4), rich in silt and clay, show lower permeability and higher water retention capacity. These soils indicate temporary hydromorphic behavior (Oyediran GO & Wakatsuki, 2015).

4.4. Analysis of the estimated water availability potential of watersheds

The estimation of water availability potential in the studied watersheds is based on an approach integrating morphometric, pedological, and statistical parameters. This analysis aims to characterize watersheds based on their capacity to retain, infiltrate, and manage runoff, depending on the interactions between morphology, soil texture, and flow dynamics (Francisco José Del Toro-Guerrero, 2018). The results in Tables 2, 8, and 9 show that the location of upstream watersheds corroborates the observations of Douha Akkari (2024), which establish a link between slopes, hydrographic networks, and a watershed's hydrological response.

ISSN: 1857-7881 (Print)
e-ISSN 1857-7431 (Online)

From a pedological perspective, soils rich in organic matter and lacking a lateritic crust serve as prime reservoirs for water retention and infiltration, unlike bowés and skeletal soils, which have limited storage capacity. The granulometric characterization confirms the presence of coarse-textured soils (fraction >50%). This soil group exhibits high hydraulic conductivity but negligible retention capacity, whereas soils dominated by fine particles offer significant surface retention despite their reduced permeability (Eléonore Beckers, 2016). The work of Askari Mohammed (2008) corroborates this analysis by demonstrating the variability of infiltration depending on soil texture and topographic position.

Multivariate analysis (PCA and CAH) validates this classification into two groups of drainage basins based on their sensitivity. On one hand, there are zones with high water availability potential (the 30 BV), corresponding to units with moderate slopes and fine textures, which correspond to hydromorphic soils. On the other hand (8BV), areas with moderate water transit are characterized by skeletal soils, where runoff predominates over infiltration (Mahyar Naseri, 2023), (Mutsa C. Masiyandima, 2025).

Conclusion

The integration of remote sensing data with Geographic Information Systems (GIS) provides an advanced approach for morphometric characterization of watersheds, differing from conventional methods. In this study, images were processed using ArcGIS and statistically analyzed to classify the watersheds of Ratoma commune based on their morphometric characteristics. Using satellite and field data, 23 morphometric parameters from 38 watersheds were analyzed, revealing two distinct hydrological groups according to their flow dynamics.Pedological characterization revealed the predominance of ferruginous and ferrallitic soils (covering approximately 75% of the study area). The granulometric properties of these soils directly control infiltration and runoff processes. Data integration made it possible to identify two mean water potential zones:

- High water potential zones, associated with hydromorphic soils
- Water transit zones, characterized by skeletal soils with rapid drainage.

This characterization constitutes a valuable decision-support tool for integrated water resources management in Ratoma. The obtained results also provide important insights for territorial planning and groundwater resource development.

Conflict of Interest: The authors reported no conflict of interest.

Data Availability: All data are included in the content of the paper.

Funding Statement: The authors did not obtain any funding for this research.

ISSN: 1857-7881 (Print)
e-ISSN 1857-7431 (Online)

References:

1. Adebisi NON, K. D. (2014). Indice et caractéristiques de résistance des sols latéritiques résiduels du sud-ouest du Nigéria. *6*(3), 229-238. doi:10.9734/BJAST/2015/7671
2. Ahmad Badruzzaman, P. W. (2025). Satellite imagery pre-processing and feature extraction for the mapping of coastal ecosystems using Google Earth Engine: A workflow for practitioners. *MethodsX, 15*, 103516. doi:10.1016/j.mex.2025.103516
3. Ameur N., e. S. (2020). *Utilisation d'un SIG pour l'évaluation des caractéristiques morphométriques d'un sous—bassin versant et leurs influences sur l'écoulement des eaux : Sous-bassin versant d'Oued Bou saâda-Algérie.* Mémoire de Master, Université Mohamed Boudiaf–M'sila.
4. Askari Mohammed, T. T. (2008). Caractéristiques d'infiltration des sols tropicaux basées sur les données de rétention d'eau. *Journal de la société Japonaise d'hydrologie et de ressources en eau, 21*(3), 215-227. doi:10.3178/jjshwr.21.215
5. Baba-Hamed K., B. A. (2016). Caractérisation d'un bassin versant par analyse statistique des paramètres morphométriques : Cas du bassin versant de la Tafra (Nord-ouest Algerien). *Géo-Eco-Trop*(40 (4)), 277–286. Retrieved from http://www.geoecotrop.be
6. Bentekhici N. (2006). Utilisation d'un SIG pour l'évaluation des caractéristiques physiques d'un bassin versant et leurs influences sur l'écoulement des eaux (bassin versant d'Oued El Maleh, Nord-Ouest d'Algérie). *Conférence francophone ESRI.*
7. Benzougagh, B. D. (2019). Apport des SIG et télédétection pour l'évaluation des caractéristiques physiques du bassin versant d'Oued Inaouene (Nord-est Maroc) et leurs utilités dans le domaine de la gestion des risques naturels. *American Journal of Innovative Research & Applied Sciences*. Retrieved from Iwww.american-jiras.com
8. Boothroyd, R. J. (2023). National-scale geodatabase of catchment characteristics in the Philippines for river management applications. *PLOS ONE, 18*(3). doi:10.1371/journal.pone.0281933
9. Bouroche J M & Saporta G. (1980). *L'analyse des données* (4ème ed.). Paris: Collection Que sais-je?
10. BRGM & ANTEA. (2014). *Assistance technique pour l'évaluation et la cartographie de l'aléa inondations en Polynésie française* . Orléan: Bureau de Recherches Géologiques et Minières.
11. Busico Gianluigi, C. N. (2020). Evaluating SWAT model performance, considering different soils data input, to quantify actual and future runoff susceptibility in a highly urbanized basin. *Journal of*

ISSN: 1857-7881 (Print)
e-ISSN 1857-7431 (Online)

Environmental Management, 110-625. doi:10.1016/j.jenvman.2020.110625

12. Centre et Réseau des technologies climatiques (CTCN). (2017). *Étude prospective des impacts du changement climatique sur la région urbaine de Conakry en vue d'une planification climato-compatible.* Conakry.
13. Chapuis Robert P. & Aubertin Michel. (2003). *Predicting the coefficient of permeability of soils using the Kozeny-Carman equation.* École polytechnique de Montréal Montréal. Retrieved from https://www.academia.edu/download/80339256/rt2003-03.pdf
14. Chirala U, K. N. (2012). Correlation of geomorphometric parameters for the hydrological characterization of Meghadrigedda watershed, Visakhapatnam, India – a GIS approach. *International Journal of Engineering Science and Technology (IJEST), 4*(07). doi:3169-3183
15. Cloutier V, L. R. (2008). Multivariate statistical analysis of geochemical data as indicative of the hydrogeochemical evolution of groundwater in a sedimentary rock aquifer system. *J. Hydrol*. doi:353: 294-313
16. Cyrus Omwoyo Ongaga, M. M. (2024). Urbanization and hydrological dynamics: a 22-year assessment of impervious surface changes and runoff in an urban watershed. *Frontiers in Water, 6*. doi:10.3389/frwa.2024.1455763
17. D2487-17, A. (2025). *Standard Practice for Classification of Soils for Engineering Purposes (Unified Soil Classification System).* American Society for Testing and Materials (ASTM). doi:store.astm.org
18. Dahiphale Pravin, K. S. (2024). Morphometric and Principal Component Analysis Based Approaches for Prioritization of Rupnagar Watershed of Punjab, India. *Journal of Agricultural Engineering (India), 61*(2), 202-218. doi:10.52151/jae2024612.1837
19. Desbordes Michel. (1989). Principales causes d'aggravation des dommages d'inondations par ruissellement superficiel en milieu urbanisé. *Bulletin Hydrologie Urbaine de la S.H.F*(4), 2 à 10.
20. Diop Baye Oumar, G. I. (2018). Grain Size Influence on the Compaction Aptitude and the Bearing Strength of the Gravel Lateritic Soils. *Geomaterials, 08*(04). doi:10.4236/gm.2018.84005
21. Douha Akkari. (2024). Étude de la corrélation entre les précipitations, le débit fluvial et les paramètres morphométriques dans le bassin versant d'El Bared, Liban Nord à l'aide du SIG. *VertigO - la revue électronique en sciences de l'environnement*. doi:10.4000/12mlb
22. Dzoualou Sorel Dzaba, A. L.-K. (2024). Caractérisation géotechnique, minéralogique, pétrographique et microstructurale de deux graviers

ISSN: 1857-7881 (Print)
e-ISSN 1857-7431 (Online)

latéritiques du Congo. *Journal saoudien de génie civil (SJCE), 8*(9), 200-212. doi: DOI : https://doi.org/10.36348/sjce.2024.v08i09.002

23. Echeverri-Díaz Jamilton, C.-H. Ó.-A.-H. (2022). Sensitivity of Empirical Equation Parameters for the Calculation of Time of Concentration in Urbanized Watersheds. *Water, 14*(18). doi:10.3390/w14182847
24. Eléonore Beckers, M. P. (2016). Characterization of stony soils' hydraulic conductivity using laboratory and numerical experiments. *SOIL, 2*(3), 421-431. doi:10.5194/soil-2-421-2016
25. Faidance Mashauri, M. M. (2023). Utilisation du système d'information géographique et modèle numérique de terrain dans l'analyse des caractéristiques hydro-morphométriques des sous-bassins versants de la rivière Tshopo, République démocratique du Congo. *Revue Internationale de Géomatique*, 13 - 18. doi:10.32604/rig.2023.044899
26. Faideance Mashauri, M. M. (2023). Influence des paramètres hydro-morphométriques sur l'écoulement des eaux des sous-bassins versants de la Tshopo, République démocratique du Congo. *Revue Internationale de Geomatique, 32*, 79-98. doi:10.32604/RIG.2023.044124
27. FAO. (2016). *Guidelines for soil description (4th edition).* Rome: FAO — Food and Agriculture Organization of the United Nations.
28. FAO. (2023). *Building Resilience into Watersheds - A Sourcebook.* Rome. doi:https://doi.org/10.4060/cc3258en
29. Faure Paul, V. B. (1998). Some factors affecting regional differentiation of the soils in the Republic of Benin (West Africa). *CATENA, 32*(3-4), 281-306. doi:10.1016/S0341-8162(98)00038-1
30. Faye Cheikh. (2014). Méthode d'analyse statistique de données morphométriques corrélation de paramètres morphométriques et influence sur l'écoulement des sous-bassins du fleuve Sénégal. *Cinq Continents, 4*(10), 80-108.
31. Francisco José Del Toro-Guerrero, E. R.-G. (2018). Variations in Soil Water Content, Infiltration and Potential Recharge at Three Sites in a Mediterranean Mountainous Region of Baja California, Mexico. *water, 10*(12), 1844. doi:10.3390/w10121844
32. Gaston C. (1942). *Dans la cendre du temps.*
33. Gaucherel C. (2003). " Pertinence de la notion d'indicateur pour la caractérisation du bassin versant". *Espace Géographique*(3), 265-281.
34. Gilbert Saporta, N. N. (2003). Analyse en composantes principales. *HAL open science*, 19-42. Retrieved from https://cnam.hal.science/hal-02507732

ISSN: 1857-7881 (Print)
e-ISSN 1857-7431 (Online)

35. Güler, C. T. (2002). Evaluation of graphical and multivariate statistical methods for classification of water chemistry data. *Hydrogeology Journal*(10), 455–474.
36. Hector Basile, C. J.-M. (2018). Hydrological functioning of western African inland valleys explored with a critical zone model. *Hydrology and Earth System Sciences, 22*(11), 5867-5888. doi:10.5194/hess-22-5867-2018
37. Henson Robin K., C. R. (2001). *Reporting Practice and Use of Exploratory Factor Analysis in Educational Research Journals.*
38. Horton R. E. (1932). Erosional development of streams and their drainage basins: Hydrophysical approach to quantitative morphology. *Bulletin of the Geological Society of America, 56*(3), 275-370. doi:10.1130/0016-7606(1945)56[275:EDOSAT]2.0.CO;2
39. Horton Robert E. (1945). Erosional development of streams and their drainage basins: Hydrophysical approach to quantitative morphology. (G. S. (GSA), Ed.) *Bulletin of the Geological Society of America, 56*(3), 275 – 370. Doi:https://doi.org/10.1130/0016-7606(1945)56%5B275:EDOSAT%5D2.0.CO;2
40. Kadéba Abel, T. S. (2020). État et propriétés des sols sous quelques espèces ligneuses des glacis dégradés du nord du Burkina Faso. *Journal d'agriculture expérimentale internationale, 42*(11), 10-22. doi:10.9734/jeai/2020/v42i1130617
41. Kirsten Hennrich, M. J. (2004). A hillslope hydrology approach for catchment-scale slope stability analysis. *Earth Surface Processes and*
42. Kouassi Amani Michel. (2021). Characterization of a potential modification of the rainfall-runoff relationship in West Africa: the case of the N'zi (Bandama) watershed in Côte d'Ivoire, Doctoral Thesis, University of Cocody-Abidjan, Côte d'Ivoire. *Physio-Géo. Géographie physique et environnement, 4*. doi:10.4000/physio-geo.1163
43. Lakraa, S. (2022). *Contribution à l'étude hydrologique du bassin versant d'Ain Smen, Fès* . Université Sidi Mohamed Ben Abdellah de Fes, Maroc.
44. Le Xuan Kham. (2008). *Variability of hydrological processes involved in the mechanism of flood generation in rapidly kinetic basins.* Toulouse: Institut National Polytechnique Toulouse. Retrieved from https://hal.science/tel-04485515v1
45. Léréyaha Coulibaly, O. M. (2025). Hydromorphological and Morphometric Analysis of the Comoé River Basin (Côte d'Ivoire): Implications for Runoff and Erosion Processes. *GSC Advanced Research and Reviews, 25*(1), 216-234. Doi:10.30574/gscarr.2025.25.1.0312

ISSN: 1857-7881 (Print)
e-ISSN 1857-7431 (Online)

46. López-Pérez Adolfo, &. F.-R. (2021). Watershed prioritization using morphometric analysis and vegetation index: a case study of Huehuetan river sub-basin, Mexico. *Arabian Journal of Geosciences, 14*(18), 18-52. doi:10.1007/s12517-021-08212-x
47. Manning Robert. (1891). On the flow of water in open channels and pipes. (I. o. Ireland, Ed.) *Transactions of the Institution of Civil Engineers of Ireland, 20*(2), 161–207.
48. Michel Lang, É. S. (2015). *L'eau à découvert.* (A. E. al., Ed.) Paris: CNRS Éditions. doi:2025-12-10 14:31:40
49. Mutsa C. Masiyandima, N. v. (2025). The hydrology of inland valleys in the sub-humid zone of West Africa: Rainfall-runoff processes in the M'b?? experimental watershed . *ResearchGate, 17*(6), 1213 - 1225. doi:10.1002/hyp.1191
50. Oyediran GO & Wakatsuki, T. (2015). Hydromorphic soils of two inland valley swamps in the rain forest zone of Nigeria. I some physical and chemical Properties. Retrieved from https://agris.fao.org/search/en/providers/125705/records/68b6dc9268d9e6806700ab3e?utm_source=chatgpt.com
51. Pearson Karl. (1901). On lines and planes of closest fit to systems of points in space. *Philosophical Magazine, 2*(11).
52. Polidori L. (1997). *" Cartographie Radar "* . Taylor & Francis,.
53. Pulido-Bosch A., C. J. (1999). Application of Principal Components analyse to the study of CO2 – rich thermaineral waters in the aqufère system of alto Guadalentin (spain). *J. Hydrologie*(46). doi:929-942
54. Sarita Gajbhiye Meshram, S. K. (2017). Prioritization of watershed through morphometric parameters : a PCA-based approach. *Applied Water Science, 7*(3), 1505-1519. doi:10.1007/s13201-015-0332-9
55. Schumm S.A. (1956). Evolution of Drainage Systems and Slopes in Badlands at Perth Amboy, New Jersey. *Bulletin of the Geological Society of America, 57*(5), 597-646. doi:10.1130/0016-7606(1956)67[597:EODSAS]2.0.CO;2
56. Sorre Maximilien. (1934). *Méditerranée. Péninsules méditerranéennes. A. Première partie. Généralités. Espagne — Portugal.* (L. A. Colin, Ed.) Paris.
57. Steffen Beck-Broichsitter, Z. H. (2023). Effet de la teneur en gravier sur les caractéristiques de rétention d'eau et la capacité thermique des sols sableux et limoneux. *Journal d'hydrologie et d'hydromécanique, 71*(1), 1-10. doi:10.2478/johh-2023-0001
58. Strahler A. N. (1952). "Hypsometric (area-altitude) analysis of erosional topography." Bull. *Bull Geol. Soc. Am.*(63), 1117–1142.

ISSN: 1857-7881 (Print)
e-ISSN 1857-7431 (Online)

59. Strahler A. N. (1957). Quantitative analysis of watershed geomorphology. *Transactions American Geophysical Union , 38*(6), 913–1920.
60. Stuti Chaudhary, A. C. (2021). Priorisation des bassins versants par analyse en composantes principales (ACP) basée sur la modélisation du ruissellement et l'évaluation de la gravité de la sécheresse dans certaines parties du bassin de la rivière Koel, Jharkhand (Inde). *Water Supply, 22*(2), 2034-2054. doi:10.2166/ws.2021.297
61. Sylla Morciré. (1995). *Processus d'alimentation de la nappe phréatique et géochimie des nitrates des eaux souterraines de la Presqu'île de Kaloum, Conakry-Guinée.* Université d'Ottawa, Ottawa: Direction des acquisitions et des services bibliographiques, 395, rue Wellington Ottawa, K1A 0N4.
62. UNESCO-IHP. (1973). *Design of water resources projects with inadequate data.* Studies and reports in hydrology, Madrid. Retrieved from http://waterscience.org
63. USGS. (2019, 06 8). *École des sciences de l'eau.*
64. Víg Balázs, F. S. (2022). Morphometric analysis of low mountains for mapping flash flood susceptibility in headwaters. *Natural Hazards, 114*(3), 3235-3254. doi:10.1007/s11069-022-05513-6